

## Article

# Nanocrystallization Effectively Improves the Oral Efficacy of an Antileishmanial Chalcone

Maria Paula Gonçalves Borsodi <sup>1</sup>, Wallace Pacienza-Lima <sup>1</sup>, Jaqueline Correia Villaça Menezes <sup>2</sup>, Douglas Escrivani-Oliveira <sup>1</sup>, Natalia Arruda-Costa <sup>1</sup>, Alcides José Monteiro da Silva <sup>3</sup>, Lucio Mendes Cabral <sup>2</sup>, Patrick G. Steel <sup>4</sup>, Ariane de Jesus Sousa-Batista <sup>1,5,\*</sup> and Bartira Rossi-Bergmann <sup>1</sup>

- <sup>1</sup> Institute of Biophysics Carlos Chagas Filho, Federal University of Rio de Janeiro, Rio de Janeiro 21941-902, Brazil; mariapaula@biof.ufrj.br (M.P.G.B.); wallace.pacienza@gmail.com (W.P.-L.); douglasescrivani@gmail.com (D.E.-O.); nataliarruda22@gmail.com (N.A.-C.); bartira@biof.ufrj.br (B.R.-B.)
- <sup>2</sup> Faculty of Pharmacy, Federal University of Rio de Janeiro, Rio de Janeiro 21941-902, Brazil; jackcvm@hotmail.com (J.C.V.M.); lmcabral2@yahoo.com.br (L.M.C.)
- <sup>3</sup> Institute of Natural Products Research, Federal University of Rio de Janeiro, Rio de Janeiro 21941-902, Brazil; alcides@nppn.ufrj.br
- <sup>4</sup> Department of Chemistry, Durham University, Lower Mountjoy, South Rd, Durham DH1 3LE, UK; p.g.steel@durham.ac.uk
- <sup>5</sup> Nanotechnology Engineering Program, Alberto Luiz Coimbra Institute for Graduate Studies, and Research in Engineering—COPPE, Federal University of Rio de Janeiro, Rio de Janeiro 21941-972, Brazil
- \* Correspondence: ariane@pent.coppe.ufrj.br

**Abstract: Background/Objectives:** Cutaneous leishmaniasis (CL) is a vector-borne neglected disease that can cause permanent deformities. Current chemotherapy based on injections with toxic drugs or oral miltefosine poses many drawbacks, urging the need for new oral therapies. Here, we proposed to increase the bioavailability of NAT22, an intralesionally but not orally active antileishmanial chalcone, through nanocrystallization to promote its oral use in CL. **Methods/Results:** NAT22 nanocrystals were produced using a solvent-free green process of dry and wet milling that reduced NAT22 crystal sizes by around 1500-fold to 257 nm (nanoNAT22). Such reduction in size increased water solubility by 15-fold to 4.3 µg/mL and ensured stability in the absence of stabilizers for at least one month. Of note, nanoNAT22 in aqueous medium was more selective for parasites (SI = 35.2) than NAT22 in 1% DMSO (SI = 7.6). *Leishmania amazonensis*-infected mice treated with oral nanoNAT22 had lesion sizes and parasite loads similar to those achieved with intralesional Glucantime<sup>®</sup>, and significantly smaller than NAT22. **Conclusions:** Together, these results indicate that nanocrystallization is an effective process to render NAT22 chalcone also orally active against CL.

**Keywords:** chalcone; nanocrystals; milling; leishmaniasis



Academic Editor:  
Natasza Skalko-Basnet

Received: 31 January 2025  
Revised: 14 March 2025  
Accepted: 18 March 2025  
Published: 21 March 2025

**Citation:** Borsodi, M.P.G.; Pacienza-Lima, W.; Menezes, J.C.V.; Escrivani-Oliveira, D.; Arruda-Costa, N.; Silva, A.J.M.d.; Cabral, L.M.; Steel, P.G.; Sousa-Batista, A.d.J.; Rossi-Bergmann, B.

Nanocrystallization Effectively Improves the Oral Efficacy of an Antileishmanial Chalcone. *Pharmaceutics* **2025**, *17*, 399. <https://doi.org/10.3390/pharmaceutics17040399>

**Copyright:** © 2025 by the authors. Licensee MDPI, Basel, Switzerland. This article is an open access article distributed under the terms and conditions of the Creative Commons Attribution (CC BY) license (<https://creativecommons.org/licenses/by/4.0/>).

## 1. Introduction

Leishmaniasis is a group of neglected diseases caused by protozoans of the genus *Leishmania*. It is estimated that around 0.6 to 1 million new cases occur annually worldwide, with cutaneous leishmaniasis (CL) accounting for more than 90% of cases [1]. Although CL is not life-threatening, it can cause disfiguring skin lesions that leave life-long scars and lead to severe social stigma. Pentavalent antimonials such as Glucantime<sup>®</sup> have been the mainstay of antileishmanial treatment for decades, and amphotericin B formulations and pentamidine have been used in antimonial-resistant cases. However, these drugs are given in long courses of parenteral injections that produce serious side effects and have low patient compliance. Intralesional injections have reduced systemic side effects of antimonials

but still require repeated injections and trained medical staff for administration. Miltefosine is the only available oral drug, but it causes gastrointestinal toxicity and is contraindicated for women of childbearing age due to its teratogenicity [2]. Consequently, there is an urgent need for new oral treatments to simplify the treatment of CL [3]. Chalcones are natural products from the flavonoid family with widely reported antileishmanial activity [4–7]. Previously, we identified a chalcone extracted from *Piper aduncum* inflorescences with strong and selective activity against *Leishmania amazonensis* [8], which served as the basis for the synthesis of more active analogues like 3-nitro-2-hidroxi-4',6'-dimetoxychalcone (CH8) [9]. More recently, the 3-nitro-2',4',6'-trimethoxychalcone (NAT22, Figure 1) was synthesized with a higher yield (89%) than CH8 (18%), and a greater parasite selectivity index compared to CH8 (1489 and 317, respectively). It demonstrated improved intralesional efficacy against CL [10] and strong binding to cytosolic trypanothione peroxidase (cTXNPx), a critical parasite target [11]. To enhance patient adherence to treatment, the oral route is recommended. Therefore, we propose the administration of NAT22 chalcone via the oral route. However, NAT22's low water solubility and large crystal structures are drawbacks for its oral use.

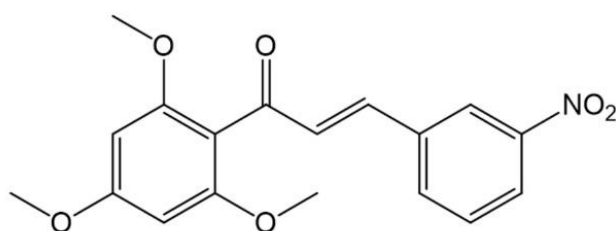


**Figure 1.** Chemical structure of NAT22 (ChemDraw).

A feasible strategy to improve drug solubility is nanocrystallization, where nanoparticles with drug alone, no lipid, or polymeric carriers have a particle size below 1  $\mu\text{m}$ . Nanocrystals offer several advantages, including increased dissolution velocity, improved adhesion to biological membranes, and enhanced absorption from the gastrointestinal tract [12,13]. Furthermore, the production of nanocrystals ensures enhanced stability in suspensions [14]. Basically, nanocrystals can be produced by three methods: top down, bottom up, or a combination of both [14]. The top-down methods of wet milling and high-pressure homogenization are normally used in products approved by the Food and Drug Administration (FDA) [15,16].

Considering the favorable crystalline nature of NAT22 and its strong therapeutic potential in leishmaniasis, this work aimed to produce NAT22 nanocrystals using a green process of dry and wet milling without the use of organic solvents to promote its oral effectiveness in leishmaniasis.

## 2. Materials and Methods

### 2.1. Materials

NAT22 chalcone was synthesized by Claisen–Schmidt condensation with 99% purity as previously described [10,17]. Analyses of the molecule are presented in the Supplementary Information. Polyvinylpyrrolidone (PVP) K30 was obtained from Labsynth (Diadema, Brazil). Polysorbate 80 was purchased from Biograde (Durham, NC, USA). Dimethyl sulfoxide (DMSO) was obtained from Sigma-Aldrich Co. (St. Louis, MO, USA). High-Performance Liquid Chromatography (HPLC)-grade solvents (acetonitrile and phosphoric acid) were purchased from Tedia (Fairfield, OH, USA). M199 and RPMI medium and heat-inactivated fetal calf serum (HIFCS) were purchased from Cultilab (Campinas, Brazil). Glucantime<sup>®</sup> (meglumine antimoniate) was obtained from Sanofi Aventis (Lyon, France).

A lactate dehydrogenase (LDH) kit was purchased from Abcam (Cambridge, UK) and a Panotipcal fast staining kit was obtained from Laborclin (Pinhais, Paraná, Brazil).

### 2.2. Preparation of nanoNAT22 Nanocrystals

NAT22 nanocrystals (nanoNAT22) were obtained by dry milling followed by wet milling of NAT22. For dry milling, a dry ball mill (Netzsch CGS 10, Selb, Germany) equipped with a 165 mL stainless steel cup and a 30 mm diameter stainless steel unit ball was used. NAT22 (2.5 g) was added to the cup and submitted to a 15 min milling cycle in dry conditions. The first step crystals—NAT22 intermediate crystals (interNAT22)—were recovered (around 80%) by scraping and then submitted to wet milling using a bench top batch mill (Netzsch PE 075, Selb, Germany) equipped with a 600 mL zirconium ceramic cup containing 0.9–1.1 mm diameter zirconium oxide beads (half milling chamber volume) stabilized with cerium oxide (CeraBeads® 1.0, Netzsch, Selb, Germany), as previously described [18]. Briefly, the obtained dry crystals (0.2% *w/v*) were dispersed in 280 mL of Milli-Q water containing 0.1% (*w/v*) PVPK-30 and 0.6% (*p/v*) of polysorbate 80, added to the milling cup with the beads, and stirred at 1700 rpm at 2 °C for 3 h. Then, the whole cup content was sieved through a #40 mesh (0.43 mm), and the sieve and beads were thoroughly washed with distilled water. The filtrate (nanocrystals) was ultracentrifuged (10,000 rpm/1 h) in Thermo Sorvall type WX Ultra (Thermo Fisher Scientific, Waltham, MA, USA) three times with distilled water to remove the surfactants. The sediment was resuspended in 5 mL of distilled water and dried in a glass petri dish at 50 °C/15 h. The obtained yellow nanocrystals were named nanoNAT22. NanoNAT22 and NAT22 were stored at room temperature in a light-protected desiccator jar until use.

### 2.3. Particle Size and Zeta Potential Analysis

NAT22, interNAT22 and nanoNAT22 were resuspended in distilled H<sub>2</sub>O (0.01% *w/v*) and dispersed by ultrasonication (UP100H, Hielscher Ultrasonics, Teltow, Germany) for 1 h. While the mean size and polydispersity index (PDI) of NAT22 was determined by laser diffraction using a Mastersizer 2000 (Malvern Panalytical, Malvern, Worcestershire, UK) [10], the interNAT22 and nanoNAT22 dispersions were diluted 1:5 in propylene glycol (5% *v/v*) and analyzed by dynamic light scattering (DLS) using a Nano Zetasizer S90 (Malvern Panalytical, Malvern, Worcestershire, UK) [19]. For zeta potential analysis, nanocrystals were resuspended in distilled water (0.1% *w/v*) and analyzed using a Zetasizer Advance Lab Blue ZSU3100 (Malvern Panalytical, Malvern, Worcestershire, UK) equipment [20].

### 2.4. Scanning Electron Microscope

Crystal morphology was imaged by scanning electron microscopy (SEM, JSM-6460/LV, JEOL, Tokyo, Japan) [20]. For that, NAT22 and nanoNAT22 powders were dispersed over double face carbon ribbons and coated with gold.

### 2.5. X-Ray Diffraction Analyses

Their crystallinity was confirmed by X-ray diffraction using an XRD-6100 diffractometer (Shimadzu, Kyoto, Japan) set to 40 kV of power, 30 mA of current, using CuK $\alpha$  radiation as an X-ray source, at 1.5418 Å wavelength, and diffraction angle scanning in a 2 $\theta$  range of 2–80° [18].

### 2.6. Fourier-Transform Infrared Spectroscopy

To evaluate the occurrence of changes in chemical bonds by milling, NAT22, interNAT22 and nanoNAT22 were mixed with KBr and analyzed by Fourier-transform infrared

spectroscopy (FTIR) using IR PRESTIGE-21 (Shimadzu, Kyoto, Japan) in the region between 4000 and 400  $\text{cm}^{-1}$  [18].

### 2.7. Water Solubility

Solubility was performed using the Shake Flask method [12]. Supersaturated solutions of NAT22 and nanoNAT22 in distilled water were ultrasonicated for 10 min using a Hielscher UP100H sonicator operating at 50% amplitude. After magnetic stirring at 200 rpm overnight, approximately 2 mL of the separation was removed and centrifuged at 10,000 rpm for 30 min. The samples were filtered with syringe filter (pore size 0.45  $\mu\text{m}$ , Merck-Millipore, Ireland) and analyzed by HPLC with an ultraviolet detector (UV-HPLC, Prominence, Shimadzu, Kyoto, Japan).

### 2.8. HPLC Analysis

NAT22 analysis was performed on a Shim-pack VP-ODS (250  $\times$  4.6 mm, with particle size of 4.6  $\mu\text{m}$ ) reverse phase column in conditions of isocratic mobile phase containing acetonitrile: 0.01% phosphoric acid (80:20  $v/v$ ) with a flow rate of 1 mL/min, detection at a wavelength of 320 nm and retention time of 4.4 min (running time: 7 min), as previously established [20]. A standard calibration curve was built up by using working standard solutions. Calibration graphs were plotted according to the linear regression analysis, with a high correlation coefficient value ( $R^2 = 0.9991$ ).

### 2.9. Particle Size Stability

NAT22 (0.01%  $w/v$ ) NAT22 and nanoNAT22 were dispersed in distilled water containing azide (2%  $w/v$ ), ultrasonicated as above, and protected from light at 26  $^{\circ}\text{C}$  for 30 days. After different time points, samples were analyzed for size by DLS (Malvern (Malvern Instruments, Malvern, Worcestershire, UK)).

### 2.10. Particle Size Dispersibility

NAT22 and nanoNAT22 were suspended at 2 mg/mL in distilled  $\text{H}_2\text{O}$  and stirred at 200 rpm overnight. After that, their absorbance,  $D$ , 274 nm) was analyzed every 5 min for 60 min using a SPECTRAMAX M5 spectrofluorometer (SpectraMax M5, Molecular Devices, San Jose, Silicon Valley, CA, USA) [21]. At the end of the analysis, macroscopic photos of the dispersions were taken.

### 2.11. In Vitro Assays

#### 2.11.1. Cell Culture

*Leishmania amazonensis* (strain WHOM/BR/75/JOSEFA) and *L. amazonensis*—GFP transfected with the green fluorescent protein (GFP) [22] were cultured at M199 medium supplemented with 10% HIFCS. Bone marrow-derived macrophages (BMDMs) were obtained as described in a previous study [23]. Briefly, cells were differentiated in vitro with L929 cell-conditioned media (LCCM) for 7 days. BMDMs were cultured at RPMI 1640 medium.

#### 2.11.2. Antipromastigote Activity

*L. amazonensis* promastigotes ( $4 \times 10^5$ /mL) were plated with medium + 5% HIFCS in 96-well culture plates in the presence of different concentrations (0.4; 2; 10; 50  $\mu\text{M}$ ) of drugs for 72 h at 26  $^{\circ}\text{C}$ . NAT22 and nanoNAT22 were directly diluted in M199 prior to addition to parasite cultures. Alternatively, NAT22 and Pentamidine isethionate (Sigma-Aldrich) were pre-diluted in 100% DMSO (Sigma-Aldrich) before addition to cultures (1% DMSO final concentration) [10]. In the last four hours of incubation, resazurin (126  $\mu\text{g}/\text{mL}$ , Sigma-Aldrich) was added to each well. At the end, the fluorescence was measured in Microplate

Spectrofluorometer (SpectraMax M5, Molecular Devices, San Jose, Silicon Valley, CA, USA) at 555 nm of excitation and 585 nm of emission. Results are represented as the half-maximal inhibitory concentration (IC<sub>50</sub>).

### 2.11.3. Antiamastigote and Macrophage Cytotoxicity Assays

For antiamastigote activity, BMDMs were allowed to adhere to glass coverslips in a 24-well plate at  $2 \times 10^5$  cells/well for 24 h/37 °C/5% CO<sub>2</sub> and then infected with *L. amazonensis* promastigotes (1:10 ratio) in M199 medium plus 5% HIFCS, for 4 h. After washing away non-internalized parasites and during 24 h. After this, cells were treated for 48 h with different concentrations (0.4; 2; 10 and 50 µM) of NAT22, nanoNAT22, or Glucantime®. NAT22 was pre-diluted in 100% DMSO before addition to cultures (1% DMSO of final concentration). At the end of treatment, coverslips were stained with Fast Panoptic macrophages and parasites were counted under microscope, and the results are expressed as the number of amastigotes/100 macrophages. For cytotoxicity, the supernatants of BMDM treated as above were colorimetrically assayed for LDH according to the manufacturer (Abcam, Cambridge, UK) instructions. The % LDH release was calculated according to Equation (1). The basal release was cells in medium alone, and maximal release was cells added with 2% Triton [10,20]. The results are expressed as the half maximal cytotoxic concentration (CC<sub>50</sub>), the concentration where the LDH release was 50%.

$$\% \text{ LDH} = \frac{(\text{OD test release} - \text{OD basal release})}{(\text{OD maximum release} - \text{OD basal release})} \times 100 \quad (1)$$

The selectivity Index (SI) considers how much more selective the treatment is for the parasite than for the cell, calculated according to Equation (2).

$$\text{SI} = \frac{\text{CC}_{50}}{\text{IC}_{50} \text{ amastigotes}} \quad (2)$$

## 2.12. In Vivo Study

### 2.12.1. Animals

BALB/c mice (females, 8-week-old) were maintained in a controlled temperature (25 °C), filtered air, 12 h light cycle and given filtered water and commercial food ad libitum throughout the experiments. The protocols using mice were approved by the Federal University of Rio de Janeiro Institutional Animal Care and Use Committee with protocol number CAUAP118.

### 2.12.2. Efficacy Against CL

BALB/c mice were infected in the ear with  $2 \times 10^6$  *L. amazonensis*-GFP promastigotes. After 8 days of infection, treatment was started with NAT22 and nanoNAT22 dispersed in polyethylene glycol at a dose of 40 mg/kg (800 µg/100 µL), administered orally by intragastric gavage, 5 times a week for 5 weeks. Glucantime® was injected subcutaneously into the infected ear at 1.5 mg/kg (30 µg Sb/10 µL), 1 × per week for 5 weeks. Periodically, animals were weighted for determination of body weight gain, and the ear thicknesses measured with a digital caliper (Mitutoyo, São Paulo, Brazil) for determination of lesion sizes that are expressed as the difference in thickness relative to the uninfected ear. Parasite loads were determined one week after treatment withdrawal (day 52) both by fluorimetry and by limiting dilution assay (LDA), as previously described [24,25].

### 2.13. Statistical Analysis

The results were analyzed by Student *t*-test (solubility) and two-way ANOVA (anti-amastigote and in vivo efficacy). Data are expressed as means  $\pm$  standard deviation (SD) for in vitro assays and means  $\pm$  standard error of the mean (SEM) for in vivo efficacy. Differences were considered significant when  $p < 0.05$ . IC<sub>50</sub> and CC<sub>50</sub> values were obtained through non-linear regression with 95% confidence intervals using GraphPad Prism<sup>®</sup> 7 and 8 software.

## 3. Results and Discussion

### 3.1. Morphology and Size of NAT22 Nanocrystals

Chalcones are known for their high crystallinity. Despite their widely described biological activities, the presentation as large crystals when in aqueous solutions hampers their therapeutic use as oral drugs [26]. Chalcone NAT22 has large crystals with a mean diameter of 400  $\mu\text{m}$  and a wide size distribution (d<sub>10</sub> = 210  $\mu\text{m}$ ; d<sub>50</sub> = 309  $\mu\text{m}$ ; d<sub>90</sub> = 888  $\mu\text{m}$ ), with a span = 2.2 (Figure 2A,B and Table 1).

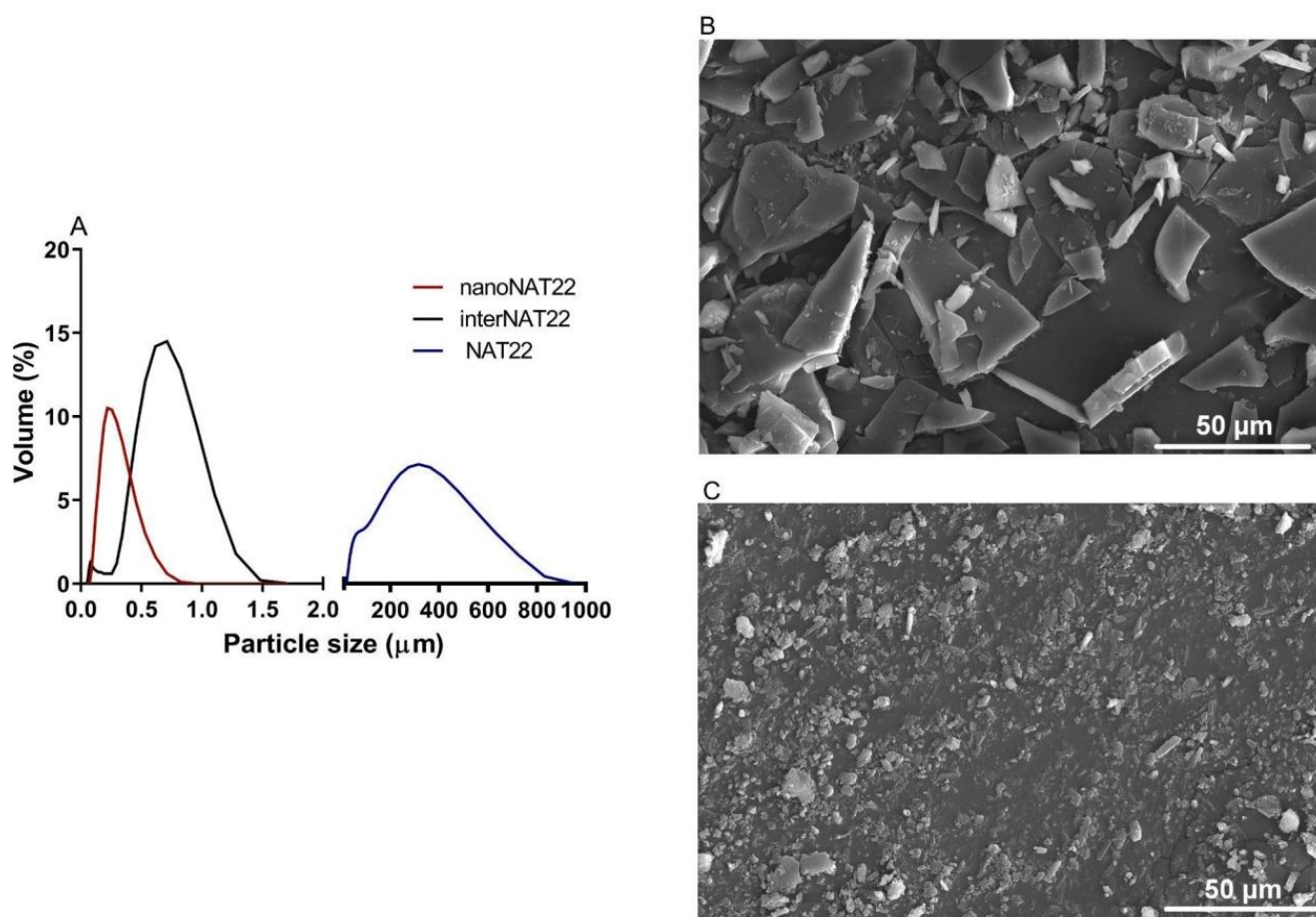


**Figure 2.** Size distribution and topography of NAT22 crystals. (A) Size polydispersion as determined by DLS (interNAT22 and nanoNAT22) and laser diffraction (NAT22). SEM images of (B) NAT22; (C) nanoNAT22. Size bars are 50  $\mu\text{m}$ .

**Table 1.** Particle size, polydispersity (PDI and span), and surface charge of NAT22 and nanocrystals.

Sample	Particle Size ( $\mu\text{M}$ )	PDI	Span	ZP (mV)
NAT22	$225 \pm 65$	NA *	$2.2 \pm 0.2$	$-2.3 \pm 3.3$
interNAT22	$0.701 \pm 0.05$	$0.5 \pm 0.03$	NA *	$-7.5 \pm 2.1$
nanoNAT22	$0.257 \pm 0.01$	$0.3 \pm 0.04$	NA *	$-24.6 \pm 2.9$

Means  $\pm$  SD (n = 3); \* NA: not applicable; ZP: zeta potential.

Based on this, the two-step dry milling plus wet milling was approached to obtain nanoNAT22. These are green processes, without the addition of organic solvents. They were carried out on a small scale but are fully industrialized technology [27]. Dry milling normally limits the size reduction to a few micrometers [28]. In dry milling, the intermediate sample interNAT22 was produced with a size around 700 nm and PDI of 0.5 (Figure 2A; Table 1). This result exceeded our expectation, since in the literature, 88  $\mu\text{m}$  crystals were obtained for ibuprofen using this technique [29]. Despite the favorable size and unimodal profile, interNAT22 presented a wide size distribution, with a PDI value  $> 0.3$ .

Therefore, it was necessary to perform wet milling to produce nanocrystals in the nanometer size range (200–500 nm) and homogeneous distribution ( $\text{PDI} \leq 0.3$ ) [15]. In this technique, the size reduction is attributed to mechanical friction and self-friction [30]. NanoNAT22 (dry + wet milling products) had a size of 257 nm and PDI of 0.3 (Figure 2A,C; Table 1), indicating that the milling process was efficient in producing monodisperse nanocrystals, compatible with the unimodal distribution seen in Figure 2A. The process was able to reduce the crystal size by about 1500 times (NAT22 = 400  $\mu\text{m}$  and nanoNAT22 = 257 nm); efficient results in the reduction of nanocrystals were also found for naproxen nanocrystals by wet milling for 1 h, which were reduced by about 500 times [31]. The size of NAT22 was reduced more times, but this depends on the crystal size of the drug. Our wet milling process was conducted in 3 h. According to zeta potential, dry + wet milling made the sample more negatively charged (around 11 times), which increases its stability due to electrostatic repulsion between the particles (Table 1) [12].

### 3.2. Chemical Stability and Crystallinity of NAT22 Chalcone

The milling process of nanopharmaceuticals should not alter the physicochemical parameters of the molecule [14]. NAT22, interNAT22, and nanoNAT22 were analyzed by FTIR to evaluate possible changes in chemical stability and crystallinity promoted by the milling processes [32]. Figure 3 shows that the three samples (NAT22, interNAT22, and nanoNAT22) presented the same band pattern, regardless of the milling process, indicating that there was no change in the molecule chemical structure (Figure 3A). The main bands of the chalcone groups can be observed in the three samples before and after grinding, with 1250 and 1040  $\text{cm}^{-1}$  bands referring to the phenyl alkyl ether group (Figure 3A, red line), and 1600–1530  $\text{cm}^{-1}$  and 1390–1300  $\text{cm}^{-1}$  referring to nitro vibrations [33]. Another band, corresponding to the C=O axial deformation vibration of the  $\alpha,\beta$ -unsaturated carbonyl, is expected to be observed in the spectrum within the region of 1625 to 1650  $\text{cm}^{-1}$  [33]. The absence of this band cannot be attributed to the milling process, as there is no specific band for the  $\alpha,\beta$ -unsaturated carbonyl in the three samples.

In the X-Ray diffractogram shown in Figure 3B, all samples have peaks with similar angles, indicating that the milling did not affect chalcone crystallinity. NAT22 peaks are around 10°, 17°, and 27°, and the same remained after milling [34]. The lower intensity of the peaks may be due to less exposure to X-rays associated with a reduction in crystal size, as seen with other nanocrystals [35–37].

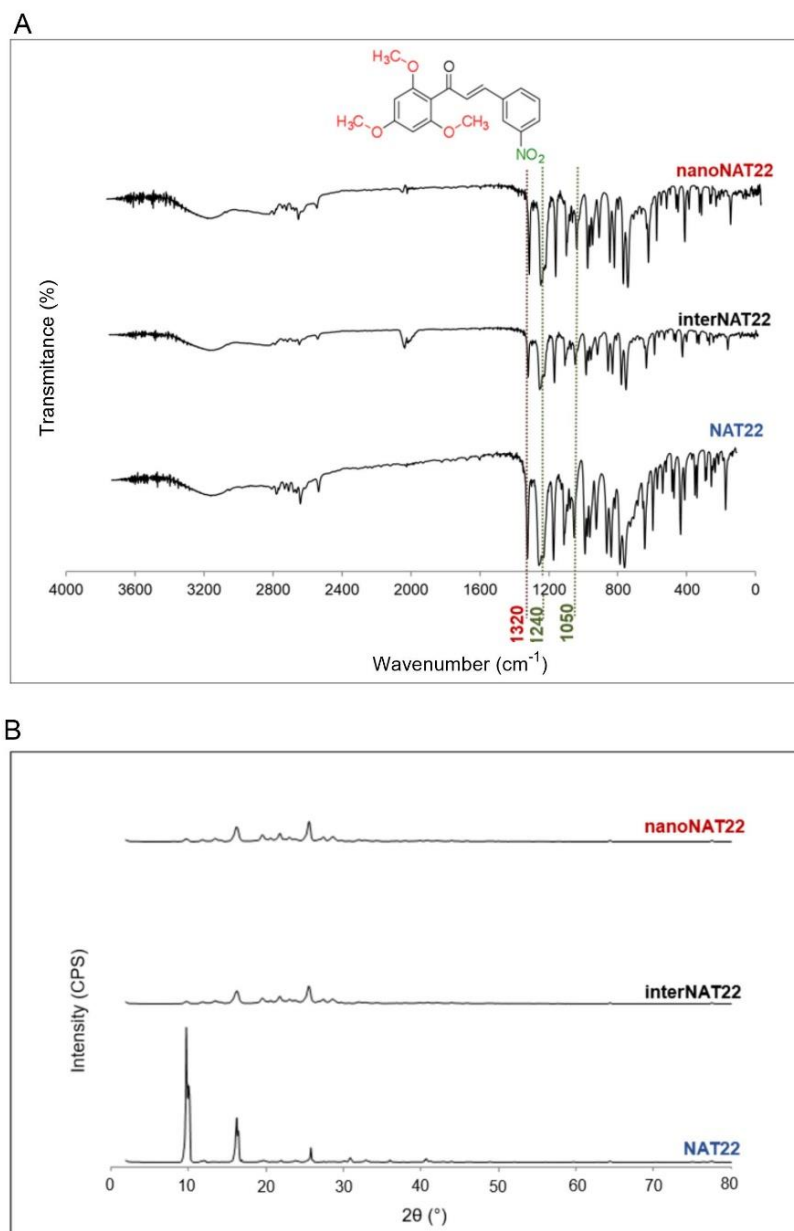


**Figure 3.** Chemical stability and crystallinity of NAT22 crystals. NAT22, interNAT22, and nanoNAT22 were compared by (A) Fourier-transform infrared spectroscopy (FTIR) for chemical stability; and (B) X-ray diffraction (XRD) for crystallinity. CPS: counts per second.

### 3.3. Solubility, Dispersibility, and Stability of NAT22 Crystals

Nanocrystallization is an excellent approach for improving drug solubility due to the larger surface area of the crystals and consequently higher saturation solubility, faster dissolution rate, and increased stability. This concept is explained by the Noyes–Whitney and Ostwald–Freundlich equations [14,16,38]. Nanomilling increased the aqueous solubility of nanoNAT22 (4.4  $\mu\text{g}/\text{mL}$ ) by 15 times compared to NAT22 (0.3  $\mu\text{g}/\text{mL}$ ) (Figure 4A). Similar increases in solubility have been observed in other studies involving the milling process, such as those with silybin and diclofenac acid nanocrystals [12,39]. The measured solubility of NAT22 solubility matched the theoretical solubility of 0.253  $\mu\text{g}/\text{mL}$  as predicted by small-molecule pharmacokinetic models (pkCSM) [40]. Despite the gain in solubility, nanoNAT22 still did not meet FDA standards (practically insoluble), so crystal dispersibility was also analyzed. NanoNAT22 showed greater dispersion stability when compared to NAT22, remaining with the same OD even after 60 min of analysis, while NAT22 quickly

precipitated (Figure 4B,C) [18]. These results show the stability of nanoNAT22 nanocrystals in water as colloidal dispersion [16]. The stability of NAT22 in aqueous suspension was further evaluated by size and PDI over 30 days at room temperature, protected from light. A small increase in crystal size and PDI was observed from day 3 onwards, likely due to the Ostwald Ripening phenomenon, where larger particles grow by aggregating smaller particles [41]. After one month, the size slightly increased to 850 nm, remaining within the nanometric range, even in the absence of stabilizers, unlike diosgenin nanocrystals, which require the combination of pluronic F127 and sodium dodecyl sulfate for one-month stability [36]. Optimizing the formulation of nanocrystals with surfactants might further increase stability. Overall, nanoNAT22 nanocrystals proved to be stable in water, with slight improvement in solubility and significant improvement in dispersion.

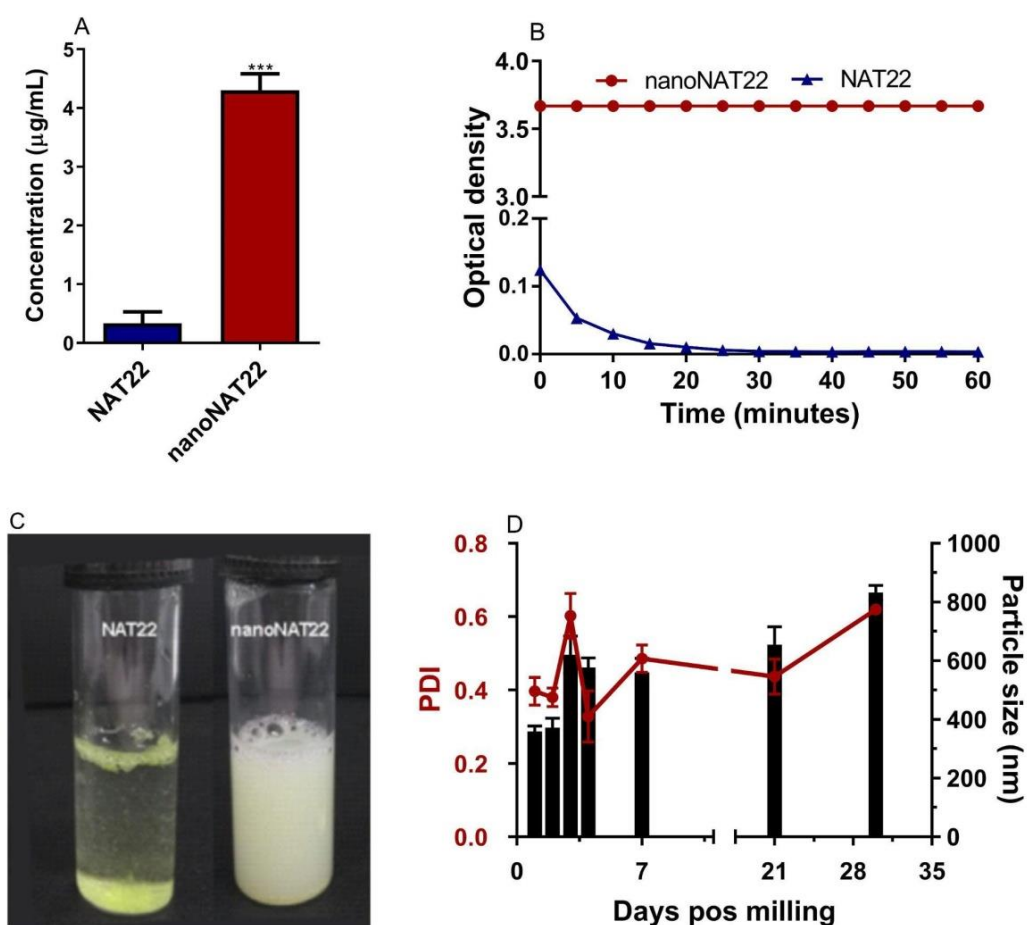


**Figure 4.** Aqueous solubility, dispersibility, and stability analysis of NAT22 crystals. (A) Solubility in water was determined by equilibrium method (shake-flask technique); (B) dispersibility was measured by optical density at the indicated times of resting after stirring; (C) images of NAT22 (left) and nanoNAT22 (right) suspensions after 60 min of resting; (D) variation in size (black) and polydispersion (red) of nanoNAT22 over time. \*\*\*  $p < 0.001$  in relation to NAT22 in water.

### 3.4. Anti-Leishmania Activity of NAT22 Crystals

Encouraged by the increased dispersibility and solubility of nanocrystals in water, we compared the antileishmanial activity of NAT22 and nanoNAT22 dispersed in M199 culture medium. The low solubility and dispersibility of NAT22 accounted for the large variation in anti-promastigote  $IC_{50}$  values ranging from 1.2  $\mu M$  to 28  $\mu M$  in three different experiments (Figure 5A and Table 2). As expected, the nanomilling process improved the anti-promastigote activity, with nanoNAT22 in the M199 medium giving a much more reproducible  $IC_{50}$  (0.7  $\mu M$ ). Significantly, this was 19 times higher than NAT22 in the same

medium ( $IC_{50} = 13 \mu\text{M}$ ). Moreover, the  $IC_{50}$  of nanoNAT in the M1199 medium was similar to that of fully soluble NAT22 in 1% DMSO ( $IC_{50} = 0.4 \mu\text{M}$ ). Importantly, similar results of anti-promastigote activity are observed for NAT22 chalcone as a control [11].

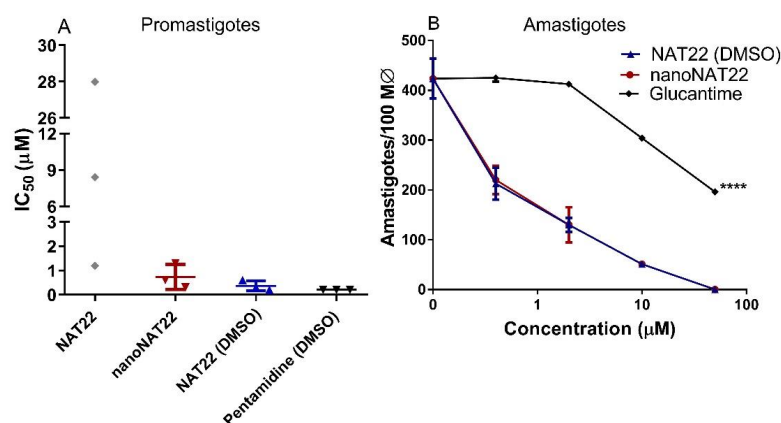


**Figure 5.** Antileishmanial activity. (A) Promastigotes were incubated with different concentrations of drugs for 72h, when parasite viability was fluorometrically determined by resazurin assay. The indicated drugs were directly diluted in aqueous medium in different concentrations, or pre-diluted in DMSO prior to addition to culture maintaining 1% DMSO (NAT22 DMSO and Pentamidine DMSO). Results are expressed as  $IC_{50}$  of three independent experiments. (B) Intracellular amastigotes were incubated with the indicated drug concentrations for 48h when the cells were stained, counted under microscope, and expressed as amastigotes/100 macrophages. Means  $\pm$  SD ( $n = 3$ ), \*\*\*\*  $p < 0.0001$  significant in all concentrations in relation to nanoNAT22.

**Table 2.** In vitro cytotoxicity and parasite selectivity.

Drug	Culture Medium	$IC_{50}$ ( $\mu\text{M}$ )		$CC_{50}$ ( $\mu\text{M}$ )	SI
		Promastigotes	Amastigotes		
NAT22	Medium	$13.0 \pm 14.0$	ND	ND	ND
nanoNAT22	Medium	$0.7 \pm 0.5$	$0.6 \pm 0.1$	$12.3 \pm 1$	20
NAT22 (DMSO)	1% DMSO	$0.4 \pm 0.2$	$0.6 \pm 0.1$	$7.7 \pm 0.9$	13
Pentamidine (DMSO)	1% DMSO	$0.2 \pm 0.0$	ND	ND	ND
Glucantime <sup>®</sup>	Medium	ND	$28.9 \pm 0.1$	$197^*$	7

Means  $\pm$  SD ( $n = 3$ ); \* extrapolated value;  $IC_{50}$ : half-maximal Inhibitory Concentration.  $CC_{50}$ : half—maximal cytotoxic concentration. SI (selectivity index):  $CC_{50}/IC_{50}$  amastigote; ND: not determined.

As with promastigotes, the large variation in anti-amastigote activity and cytotoxicity when NAT22 was dispersed in medium alone did not allow for the establishment of  $CC_{50}$  and SI values. In the intracellular anti-amastigote assay, nanoNAT22 dispersed in the RPMI medium showed the same activity as NAT22 solution in 1% DMSO (Figure 5B), with an  $IC_{50}$  equal to  $0.6 \mu\text{M}$  (Table 2), similar to that observed with promastigotes. Despite the higher bioavailability, nanoNAT22 in the RPMI medium was 1.6 times safer ( $CC_{50} = 12.3 \mu\text{M}$ ) than NAT22 in 1% DMSO ( $CC_{50} = 7.7 \mu\text{M}$ ); similar results were found by our group for this control [11]. Considering the selectivity index (SI) ( $SI = CC_{50}/IC_{50}$  amastigote) values, the drug must be at least 10–20 times more selective to the parasite than the cell [42]. With that, nanoNAT22s were 1.5 times more selective for the parasite ( $SI = 20$  for nanoNAT22 in medium and  $SI = 13$  for NAT22 in 1% DMSO) (Table 2). This demonstrates that nanoNAT22 presents greater selectivity and it is in accordance with the defined criteria. We can also highlight the modest increase in the performance of NAT22 chalcone nanocrystals compared to hydroxymethylnitrofurazone nanocrystals prepared by wet milling, as determined by calculating the selectivity index [43].

### 3.5. Oral Efficacy of nanoNAT22 in Murine Model of Cutaneous Leishmaniasis

Nanocrystals are an excellent approach to improve drug solubility/dispersibility, favoring oral administration [28]. The choice of this route is related to greater patient acceptance due to easy administration, no requirement for sterilization, and specialized professional or hospitalization, as happens with some conventional treatments of leishmaniasis, facilitating the treatment of this neglected disease. In addition, the oral route is also in accordance with the guidelines recommended by the Drugs for Neglected Diseases initiative (DNDi) [3].

Treatment with nanoNAT22 orally demonstrated greater efficacy than NAT22 in terms of reduction in lesion sizes ( $p < 0.001$ ) and in parasite loads as evaluated by fluorimetry ( $p < 0.01$ ) and LDA that indirectly measures living parasites in the lesion (Figures 6C,D, respectively). The effectiveness of nanoNAT22 for oral route was similar to that obtained following treatment with intralesional Glucantime<sup>®</sup> in terms of reducing lesion size and parasite load (60 and 54%, respectively), and such represents a promising result for a non-invasive route (Figure 6A,C). Importantly, the treatments were not toxic and, despite an initial weight loss, by the end of the treatment all animals gained more weight than the untreated group (Figure 6B). These results demonstrate that nanocrystallization improved the effectiveness of oral chalcone in CL. Similar results have been reported for amphotericin B nanosuspensions in VL, in which a 29% greater reduction in the parasite load was seen, indicating superior oral absorption and efficacy of this formulation [44]. The improvement may be due to the greater adhesiveness of the nanocrystals to the gastrointestinal mucosa, favoring absorption and increasing the residence time in the gastrointestinal tract by increasing the solubility and dissolution of the suspension [38].

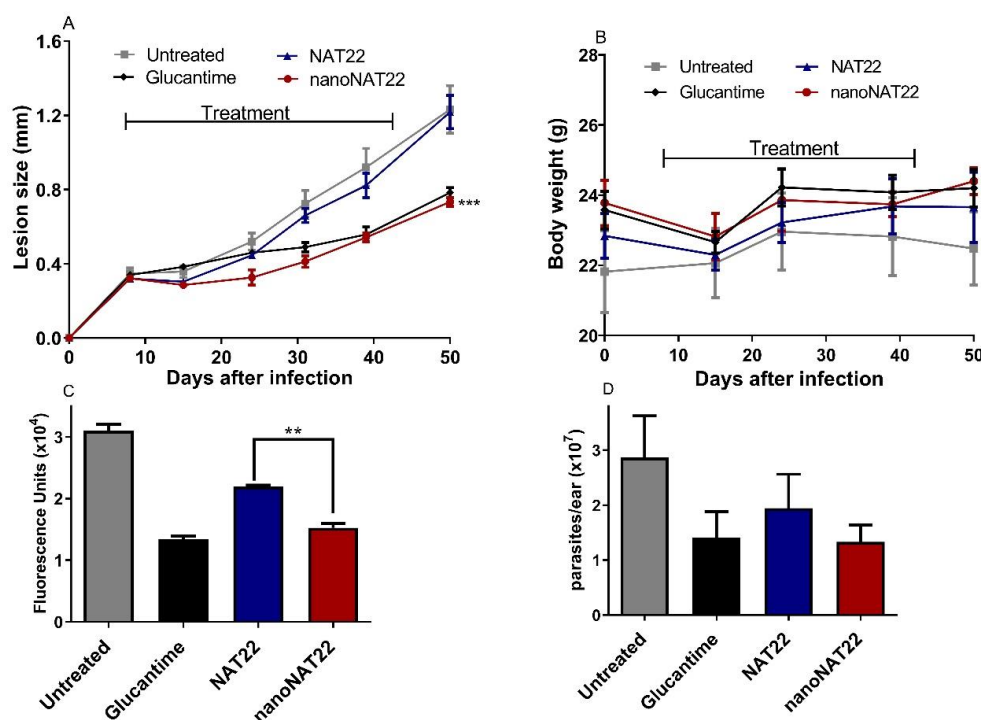


**Figure 6.** Efficacy of oral treatment with NAT22 nanocrystals in cutaneous leishmaniasis. Mice were infected with *L. amazonensis*-GFP in the ear. On day 8 of infection, they were orally administered with 40 mg/kg of NAT22 or nanoNAT22 in propylene glycol 5×/week, or intralesional injection with Glucantime<sup>®</sup> (1.5 mg/kg), 1×/week for five weeks. (A) Lesion sizes are expressed as the difference of ear thickness in relation to non-infected ears, and (B) body weights were measured on the indicated days. Parasite loads in the infected ears were determined on day 52 post infection by (C) fluorimetry, and (D) limiting dilution assay. Mean ± SEM (n = 5). \*\*  $p < 0.01$ ; \*\*\*  $p < 0.001$  in relation to NAT22.

## 4. Conclusions

The combined dry and wet milling process was efficient in producing NAT22 nanocrystals (nanoNAT22) with nanometric and homogeneous dispersion without affecting the crystallinity and chemical structure of the molecule. This process subtly improved solubility and substantially increased the dispersibility of NAT22 nanocrystals in aqueous media, keeping the nanocrystals stable and nanosized for at least 30 days in the absence of any stabilizer (size < 1  $\mu\text{m}$ ). Nanomilling proved to be an effective method to improve the bioavailability of NAT22 both in vitro and in vivo, promoting good anti-*Leishmania* activity, with a high selectivity index in an aqueous medium and an excellent efficacy of orally administered nanoNAT22. These results demonstrated that nanocrystalline NAT22 is a potent candidate for the oral treatment of cutaneous leishmaniasis.

**Supplementary Materials:** The following supporting information can be downloaded at: <https://www.mdpi.com/article/10.3390/pharmaceutics17040399/s1>, Supplementary Figure S1. Chromatogram of nanoNAT22 with detection at 320 nm. Supplementary Figure S2. Gas chromatography mass spectrometry (GC-MS). The NAT 22 purity was 99%. Supplementary Figure S3. Mass spectrometry of NAT22. EM (IE) m/z (%) 343 (20), 315 M + (100), 195 (50).

**Author Contributions:** Conceptualization: A.d.J.S.-B., B.R.-B., P.G.S. and L.M.C.; methodology: A.J.M.d.S., D.E.-O., J.C.V.M., M.P.G.B., N.A.-C., P.G.S. and W.P.-L.; formal analysis: A.d.J.S.-B., J.C.V.M., M.P.G.B. and W.P.-L.; data curation: J.C.V.M., M.P.G.B. and W.P.-L.; writing—original draft preparation, M.P.G.B.; writing—review and editing, A.d.J.S.-B., B.R.-B. and M.P.G.B.; supervision, A.d.J.S.-B. and B.R.-B. All authors have read and agreed to the published version of the manuscript.

**Funding:** This research was supported by FAPERJ Carlos Chagas Filho Foundation for Research Support of the State of Rio de Janeiro (FAPERJ) through projects E-26/201.384/2022 (JCNE) and E26/010.002426/2019 (REDE SAÚDE).

**Institutional Review Board Statement:** The animal study protocol was approved by the Federal University of Rio de Janeiro Institutional Animal Care and Use Committee with protocol number CAUAP118.

**Informed Consent Statement:** Not applicable.

**Data Availability Statement:** Data are available in the article and Supplementary Materials.

**Conflicts of Interest:** The authors declare no conflicts of interest.

## Abbreviations

The following abbreviations are used in this manuscript:

BMDM	Bone marrow-derived macrophages
CC <sub>50</sub>	Half -maximal cytotoxic concentration
CL	Cutaneous leishmaniasis
DLS	Dynamic light scattering
DMSO	Dimethyl sulfoxide
DNDi	Drugs for Neglected Diseases Initiative
FTIR	Fourier-transform infrared spectroscopy
GFP	Green fluorescent protein
HIFCS	Heat-inactivated fetal calf serum
InterNAT22	NAT22 intermediate crystals
IC <sub>50</sub>	Half-maximal inhibitory concentration
LDA	Limiting dilution assay
LDH	Lactate dehydrogenase
NA	Not applicable
NanoNAT22	NAT22 nanocrystals
NAT22	3-nitro-2',4',6'-trimethoxychalcone

ND	Not determined
OD	Optical density
SD	Standard deviation
PDI	Polydispersity index
pkCSM	Predicting small-molecule pharmacokinetic
PVP	Polyvinylpyrrolidone
SEM	Scanning electron microscopy
SEM	Standard error of the mean
SI	Selectivity index
UV-HPLC	High-Performance Liquid Chromatography with ultraviolet detector
ZP	Zeta potential

## References

- Bamorovat, M.; Sharifi, I.; Khosravi, A.; Aflatoonian, M.R.; Agha Kuchak Afshari, S.; Salarkia, E.; Sharifi, F.; Aflatoonian, B.; Gharachorloo, F.; Khamesipour, A.; et al. Global Dilemma and Needs Assessment Toward Achieving Sustainable Development Goals in Controlling Leishmaniasis. *J. Epidemiol. Glob. Health* **2024**, *14*, 22–34. [PubMed]
- Astman, N.; Arbel, C.; Katz, O.; Barzilai, A.; Solomon, M.; Schwartz, E. Tolerability and Safety of Miltefosine for the Treatment of Cutaneous Leishmaniasis. *Trop. Med. Infect. Dis.* **2024**, *9*, 218. [CrossRef]
- DNDI. Towards a New Generation of Treatments for Leishmaniasis. Available online: [https://dndi.org/wp-content/uploads/2019/09/DNDi\\_Leishmaniasis\\_2019\\_POR.pdf](https://dndi.org/wp-content/uploads/2019/09/DNDi_Leishmaniasis_2019_POR.pdf) (accessed on 10 January 2025).
- Chen, M.; Christensen, S.B.; Blom, J.; Lemmich, E.; Nadelmann, L.; Fich, K.; Theander, T.G.; Kharazmi, A. Licochalcone A, a novel antiparasitic agent with potent activity against human pathogenic protozoan species of Leishmania. *Antimicrob. Agents Chemother.* **1993**, *37*, 2550–2556.
- Yunes, R.; Chiaradia, L.D.; Leal, P.C.; Cechinel Filho, V.; Torres-Santos, E.C.; Falcão, C.A.B.; Rossi-Bergmann, B. Chalcones as new drug leads against leishmaniasis. *Curr. Trends Med. Chem.* **2006**, *4*, 47–56.
- Tajuddeen, N.; Isah, M.B.; Suleiman, M.A.; van Heerden, F.R.; Ibrahim, M.A. The chemotherapeutic potential of chalcones against leishmaniasis: A review. *Int. J. Antimicrob. Agents* **2018**, *51*, 311–318.
- Barreto, T.S.A.; Santos, T.A.C.; Silva, A.R.S.T.; Costa, E.V.; Pinheiro, L.A.; Fernandes, R.P.M.; Scher, R.; Alves, P. Brominated chalcones as promising antileishmanial agents. *Bioorganic Med. Chem. Lett.* **2025**, *116*, 130042.
- Torres-Santos, E.C.; Moreira, D.L.; Kaplan, M.A.; Meirelles, M.N.; Rossi-Bergmann, B. Selective effect of 2',6'-dihydroxy-4'-methoxychalcone isolated from Piper aduncum on Leishmania amazonensis. *Antimicrob. Agents Chemother.* **1999**, *43*, 1234–1241.
- Boeck, P.; Falcão, C.A.B.; Leal, P.C.; Yunes, R.A.; Filho, V.C.; Torres-Santos, E.C.; Rossi-Bergmann, B. Synthesis of chalcone analogues with increased antileishmanial activity. *Bioorganic Med. Chem.* **2006**, *14*, 1538–1545.
- Sousa-Batista, A.J.; Arruda-Costa, N.; Escrivani-Oliveira, D.; Reynaud, F.; Steel, P.G.; Rossi-Bergmann, B. Single-dose treatment for cutaneous leishmaniasis with an easily synthesized chalcone entrapped in polymeric microparticles. *Parasitology* **2020**, *147*, 1032–1037.
- Escrivani-Oliveira, D.; Charlton, R.; Caruso, M.; Burle-Caldas, G.; Borsodi, M.P.G.; Zingali, R.; Mello, M.V.; Jesus, J.; Souza, A.; Abraham-Viera, B.; et al. Chalcones identify cTXNPx as a potential antileishmanial drug target. *PLoS Neglected Trop. Dis.* **2021**, *15*, 11.
- Seo, S.; Kim, G.Y.; Kim, M.H.; Lee, K.W.; Kim, M.J.; Chaudhary, M.; Bikram, K.; Kim, T.; Choi, S.; Yang, H.; et al. Nanocrystal Formulation to Enhance Oral Absorption of Silybin: Preparation, In Vitro Evaluations, and Pharmacokinetic Evaluations in Rats and Healthy Human Subjects. *Pharmaceutics* **2024**, *16*, 1033. [CrossRef] [PubMed]
- Thipparaboina, R.; Chavan, R.B.; Shastri, N.R. Nanocrystals for Delivery of Therapeutic Agents. In *Particulate Technology for Delivery of Therapeutics*; Springer: Berlin/Heidelberg, Germany, 2017; pp. 291–316.
- Pardhi, V.P.; Verma, T.; Flora, S.J.S.; Chandasana, H.; Shukla, R. Nanocrystals: An Overview of Fabrication, Characterization and Therapeutic Applications in Drug Delivery. *Curr. Pharm. Des.* **2018**, *24*, 5129–5146. [CrossRef] [PubMed]
- Medarević, D.; Ibrić, S.; Vardaka, E.; Mitrić, M.; Nikolakakis, I.; Kachrimanis, K. Insight into the Formation of Glimepiride Nanocrystals by Wet Media Milling. *Pharmaceutics* **2020**, *12*, 53. [CrossRef]
- Jarvis, M.; Krishnan, V.; Mitragotri, S. Nanocrystals: A perspective on translational research and clinical studies. *Bioeng. Transl. Med.* **2019**, *4*, 5–16. [CrossRef] [PubMed]
- Amslinger, S.; Al-Rifai, N.; Winter, K.; Wörmann, K.; Scholz, R.; Baumeister, P.; Wilda, M. Reactivity assessment of chalcones by a kinetic thiol assay. *Org. Biomol. Chem.* **2013**, *11*, 549. [CrossRef]

18. Villaça, J.C.; Silva, L.C.R.P.; Locatelli, F.R.; Meireles, P.W.; Carmo, F.A.; Rodrigues, C.R.; Tavares, M.I.B.; Sousa, V.P.; Cabral, L.M. Full-factorial design for statistical planning of attritor milling parameters and evaluation of effects on particle size and structure of sodium-montmorillonite. *Eng. Res. Express* **2020**, *2*, 1. [CrossRef]
19. Meireles, P.W.; de Souza, D.P.B.; Rezende, M.G.; Borsodi, M.P.G.; de Oliveira, D.E.; da Silva, L.C.R.P.; de Souza, A.M.T.; Viana, G.M.; Rodrigues, C.R.; do Carmo, F.A.; et al. Nanoparticles Loaded with a New Thiourea Derivative: Development and In vitro Evaluation Against *Leishmania amazonensis*. *Curr. Drug Deliv.* **2020**, *17*, 694–702. [CrossRef]
20. Sousa-Batista, A.J.; Pacienza-Lima, W.; Arruda-Costa, N.; Falcão, C.A.B.; Ré, M.I.; Rossi-Bergmann, B. Depot Subcutaneous Injection with Chalcone CH8-Loaded Poly(Lactic-Co-Glycolic Acid) Microspheres as a Single-Dose Treatment of Cutaneous Leishmaniasis. *Antimicrob. Agents Chemother.* **2018**, *62*, e01822-17. [CrossRef]
21. Lin, N.; Zhao, S.; Gan, L.; Chang, P.R.; Xia, T.; Huang, J. Preparation of fungus-derived chitin nanocrystals and their dispersion stability evaluation in aqueous media. *Carbohydr. Polym.* **2017**, *173*, 610–618. [CrossRef]
22. Costa, S.S.; GOLIM, M.A.; Rossi-Bergmann, B.; Costa, F.T.M.; Giorgio, S. Use of In Vivo and In Vitro Systems to Select *Leishmania amazonensis* Expressing Green Fluorescent Protein. *Korean J. Parasitol.* **2011**, *49*, 357–364. [CrossRef]
23. Rios, F.J.; Touyz, R.M.; Montezano, A.C. Isolation and Differentiation of Murine Macrophages. *Methods Mol. Biol.* **2017**, *1527*, 297–309. [PubMed]
24. Demicheli, C.; Ochoa, R.; da Silva, J.B.B.; Falcão, C.A.B.; Rossi-Bergmann, B.; de Melo, A.L.; Sinisterra, R.D.; Frézard, F. Oral delivery of meglumine an-timoniato-beta-cyclodextrin complex for treatment of leishmaniasis. *Antimicrob. Agents Chemother.* **2004**, *48*, 100–103. [CrossRef] [PubMed]
25. Lima, H.C.; Bleyenbergh, J.A.; Titus, R.G. A simple method for quantifying *Leishmania* in tissues of infected animals. *Parasitol. Today* **1997**, *13*, 80–82.
26. Gamboa, J.M.; Leong, K.W. In vitro and in vivo models for the study of oral delivery of nanoparticles. *Adv. Drug Deliv. Rev.* **2013**, *65*, 800–810.
27. Bitterlich, A.; Mihorko, A.; Juhnke, M. Design Space and Control Strategy for the Manufacturing of Wet Media Milled Drug Nanocrystal Suspensions by Adopting Mechanistic Process Modeling. *Pharmaceutics* **2024**, *16*, 328. [CrossRef]
28. Williams, H.D.; Trevaskis, N.L.; Charman, S.A.; Shanker, R.M.; Charman, W.N.; Pouton, C.W.; Porter, C.J. Strategies to address low drug solubility in discovery and development. *Pharmacol. Rev.* **2013**, *65*, 315–499. [PubMed]
29. Kumar, D.; Worku, Z.A.; Gao, Y.; Kamaraju, V.K.; Glennon, B.; Babu, R.P.; Healy, A.M. Comparison of wet milling and dry milling routes for ibuprofen pharmaceutical crystals and their impact on pharmaceutical and biopharmaceutical properties. *Powder Technol.* **2018**, *330*, 228–238.
30. Loh, Z.H.; Samanta, A.K.; Sia Heng, P.W. Overview of milling techniques for improving the solubility of poorly water-soluble drugs. *Asian J. Pharm. Sci.* **2015**, *10*, 255–274.
31. Merisko-Liversidge, E.; Liversidge, G.G. Nanosizing for oral and parenteral drug delivery: A perspective on formulating poorly-water soluble compounds using wet media milling technology. *Adv. Drug Deliv. Rev.* **2011**, *63*, 6.
32. Jahangir, M.A.; Imam, S.S.; Muheem, A.; Chettupalli, A.; Al-Abbasi, F.A.; Nadeem, M.S.; Kazmi, I.; Afzal, M.; Alshehri, S. Nanocrystals: Characterization Overview, Applications in Drug Delivery, and Their Toxicity Concerns. *J. Pharm. Innov.* **2020**, *17*, 237–248.
33. Merck. IR Spectrum Table & Chart. Available online: <https://www.sigmaaldrich.com/technical-documents/articles/biology/ir-spectrum-table.html#ir-table-by-compound> (accessed on 15 January 2025).
34. Budziak, I.; Arczewska, M.; Kaminski, D.M. Formation of Prenylated Chalcone Xanthohumol Cocrystals: Single Crystal X-Ray Diffraction, Vibrational Spectroscopic Study Coupled with Multivariate Analysis. *Molecules* **2019**, *24*, 4245. [CrossRef] [PubMed]
35. Shah, S.M.; Ullah, F.; Khan, S.; Shah, S.M.; de Matas, M.; Hussain, Z.; Minhas, M.U.; AbdEl-Salam, N.M.; Assi, K.H.; Isreb, M. Smart Nanocrystals of Artemether: Fabrication, Characterization, and Comparative in Vitro and in Vivo Antimalarial Evaluation. *Drug Design, Development and Therapy. Drug Des. Dev. Ther.* **2016**, *10*, 3837–3850. [CrossRef] [PubMed]
36. Liu, C.Z.; Chang, J.H.; Zhang, L.; Xue, H.F.; Liu, X.G.; Liu, P.; Fu, Q. Preparation and Evaluation of Diosgenin Nanocrystals to Improve Oral Bioavailability. *AAPS PharmSciTech.* **2017**, *18*, 2067–2076. [CrossRef] [PubMed]
37. Yang, H.; Teng, F.; Wang, P.; Tian, B.; Lin, X.; Hu, X.; Zhang, L.; Zhang, K.; Zhang, Y.; Tang, X. Investigation of a Nanosuspension Stabilized by Soluplus<sup>®</sup> to Improve Bioavailability. *Int. J. Pharm.* **2014**, *477*, 88–95. [CrossRef]
38. Malamataris, M.; Taylor, K.M.G.; Malamataris, S.; Douroumis, D.; Kachrimanis, K. Pharmaceutical nanocrystals: Production by wet milling and applications. *Drug Discov. Today* **2018**, *23*, 534–547. [CrossRef]
39. Pireddu, R.; Caddeo, C.; Valenti, D.; Marongiu, F.; Scano, A.; Ennas, G.; Lai, F.; Fadda, A.M.; Sinico, C. Diclofenac acid nanocrystals as an effective strategy to reduce in vivo skin inflammation by improving dermal drug bioavailability. *Colloids Surf. B Biointerfaces* **2016**, *143*, 64–70. [CrossRef]
40. Pires, D.E.V.; Blundell, T.L.; Ascher, D.B. pkCSM: Predicting Small-Molecule Pharmacokinetic and Toxicity Properties Using Graph-Based Signatures. *J. Med. Chem.* **2015**, *58*, 4066–4072. [CrossRef]

41. Sugimoto, T. Chapter 4—Recrystallization. In *Monodispersed Particles*, 2nd ed.; Elsevier: Amsterdam, The Netherlands, 2019; pp. 167–179.
42. Don, R.; Ioset, J.R. Screening strategies to identify new chemical diversity for drug development to treat kinetoplastid infections. *Parasitology* **2014**, *141*, 140–146. [[CrossRef](#)]
43. Scarim, C.B.; de Souza, A.; Marins, D.S.S.; Santos, E.G.d.; de Figueiredo Diniz Castro, L.; Caldas, I.S.; Espuri, P.F.; Marques, M.J.; Ferreira, E.I.; Bou-Chacra, N.A.; et al. Synthesis, Characterization, and Activity of Hydroxymethylnitrofurazone Nanocrystals against *Trypanosoma cruzi* and *Leishmania* spp. *Drugs Drug Candidates* **2022**, *1*, 43–55. [[CrossRef](#)]
44. Kayser, O.; Olbrich, C.; Yardley, V.; Kiderlen, A.F.; Croft, S.L. Formulation of Amphotericin B as Nanosuspension for Oral Administration. *Int. J. Pharm.* **2003**, *254*, 73–75. [[CrossRef](#)]

**Disclaimer/Publisher’s Note:** The statements, opinions and data contained in all publications are solely those of the individual author(s) and contributor(s) and not of MDPI and/or the editor(s). MDPI and/or the editor(s) disclaim responsibility for any injury to people or property resulting from any ideas, methods, instructions or products referred to in the content.